Structural and optical properties of highly Er-doped Yb-Y disilicate thin films

Paolo Cardile,[1] Maria Miritello,[1,*] Francesco Ruffino,[1,2] and Francesco Priolo[1,2]

[1]*CNR-IMM MATIS, via S. Sofia 64, I-95123 Catania, Italy*
[2]*Dipartimento di Fisica e Astronomia, Università di Catania, via S. Sofia 64, I-95123 Catania, Italy*
**maria.miritello@ct.infn.it*

Abstract: Highly Er-doped Yb-Y disilicates thin films grown on c-Si will be presented. The approach has permitted to vary independently the concentrations of both active rare earths, Er and Yb, and to effectively control the Er sensitization from Yb ions. We will demonstrate that these films are stable, having a uniform distribution of the chemical components throughout their thickness and a favored crystallization of the α-phase, which is the most optically efficient. We verified that this crystallization can be ascribed to a densification of the material and to the mobility locally introduced by ion implantation. Finally we will show a strong PL emission at 1.54 μm, associated to the Yb-Er energy transfer mechanism, without any deleterious energy back-transfer. These properties make this new class of thin films a valuable and promising approach for the realization of efficient planar amplifiers.

©2012 Optical Society of America

OCIS codes: (230.4480) Optical amplifiers; (160.5690) Rare-earth-doped materials; (260.2160) Energy transfer.

References and links

1. H. Ennen, J. Schneider, G. Pomrenke, and A. Axmann, "1.54-μm luminescence of erbium-implanted III-V semiconductors and silicon," Appl. Phys. Lett. **43**(10), 943–945 (1983).
2. K. Kenyon, "Recent developments in rare-earth doped materials for optoelectronics," J. Prog. Quantum Electron. **26**(4-5), 225–284 (2002).
3. A. Polman, "Erbium implanted thin film photonic materials," J. Appl. Phys. **82**(1), 1–39 (1997).
4. K. Hattori, T. Kitagawa, M. Oguma, Y. Ohmori, and M. Horiguchi, "Erbium-doped silica-based waveguide amplifier integrated with a 980/1530 nm WDM coupler," Electron. Lett. **30**(11), 856–857 (1994).
5. Y. C. Yan, A. J. Faber, H. de Waal, P. J. Kik, and A. Polman, "Erbium-doped phosphate glass waveguide on silicon with 4.1 dB/cm gain at 1.535 μm," Appl. Phys. Lett. **71**(20), 2922–2924 (1997).
6. M. Miritello, R. Lo Savio, A. M. Piro, G. Franzò, F. Priolo, F. Iacona, and C. Bongiorno, "Optical and structural properties of Er_2O_3 films grown by magnetron sputtering," J. Appl. Phys. **100**(1), 013502 (2006).
7. T.-D. Nguyen, C.-T. Dinh, and T.-O. Do, "Shape- and size-controlled synthesis of monoclinic ErOOH and cubic Er_2O_3 from micro- to nanostructures and their upconversion luminescence," ACS Nano **4**(4), 2263–2273 (2010).
8. M. Miritello, R. Lo Savio, F. Iacona, G. Franzò, A. Irrera, A. M. Piro, C. Bongiorno, and F. Priolo, "Efficient luminescence and energy transfer in erbium silicate thin films," Adv. Mater. **19**(12), 1582–1588 (2007).
9. H.-J. Choi, J. H. Shin, K. Suh, H.-K. Seong, H.-C. Han, and J.-C. Lee, "Self-organized growth of Si/silica/$Er_2Si_2O_7$ core-shell nanowire heterostructures and their luminescence," Nano Lett. **5**(12), 2432–2437 (2005).
10. F. Vetrone, J. C. Boyer, J. A. Capobianco, A. Speghini, and M. Bettinelli, "Effect of Yb^{3+} codoping on the upconversion emission in nanocrystalline Y_2O_3:Er^{3+}," J. Phys. Chem. B **107**(5), 1107–1112 (2003).
11. R. Lo Savio, M. Miritello, P. Cardile, and F. Priolo, "Concentration dependence of the Er^{3+} visible and infrared luminescence in $Y_{2-x}Er_xO_3$ thin films on Si," J. Appl. Phys. **106**(4), 043512 (2009).
12. M. Miritello, P. Cardile, R. Lo Savio, and F. Priolo, "Energy transfer and enhanced 1.54 μm emission in erbium-ytterbium disilicate thin films," Opt. Express **19**(21), 20761–20772 (2011), http://www.opticsinfobase.org/oe/abstract.cfm?uri=oe-19-21-20761.
13. M. Miritello, R. Lo Savio, P. Cardile, and F. Priolo, "Enhanced down conversion of photons emitted by photoexcited $Er_xY_{2-x}Si_2O_7$ films grown on silicon," Phys. Rev. B **81**(4), 041411 (2010).

#175165 - $15.00 USD Received 28 Aug 2012; revised 13 Oct 2012; accepted 15 Oct 2012; published 29 Nov 2012
(C) 2013 OSA

14. X. J. Wang, B. Wang, L. Wang, R. M. Guo, H. Isshiki, T. Kimura, and Z. Zhou, "Extraordinary infrared photoluminescence efficiency of $Er_{0.1}Yb_{1.9}SiO_5$ films on SiO_2/Si substrates," Appl. Phys. Lett. **98**(7), 071903 (2011).
15. X. J. Wang, G. Yuan, H. Isshiki, T. Kimura, and Z. Zhou, "Photoluminescence enhancement and high gain amplification of $Er_xY_{2-x}SiO_5$ waveguide," J. Appl. Phys. Lett. **108**, 013506 (2010).
16. K. Suh, J.-H. Shin, S.-J. Seo, and B.-S. Bae, "Er^{3+} luminescence and cooperative upconversion in $Er_xY_{2-x}SiO_5$ nanocrystal aggregates fabricated using Si nanowires," Appl. Phys. Lett. **92**(12), 121910 (2008).
17. M. C. Strohhöfer and A. Polman, "Absorption and emission spectroscopy in Er^{3+}-Yb^{3+} doped aluminum oxide waveguides," Opt. Mater. **21**(4), 705–712 (2003).
18. G. C. Valley, "Modeling cladding-pumped Er/Yb fiber amplifiers," Opt. Fiber Technol. **7**(1), 21–44 (2001).
19. H. S. Hsu, C. Cai, and A. M. Armani, "Ultra-low-threshold Er:Yb sol-gel microlaser on silicon," Opt. Express **17**(25), 23265–23271 (2009), http://www.opticsinfobase.org/oe/abstract.cfm?URI=oe-17-25-23265.
20. B. Wang, R. M. Guo, X. J. Wang, L. Wang, L. Y. Hong, B. Yin, L. F. Gao, and Z. Zhou, "Near-infrared electroluminescence in ErYb silicate based light-emitting device," Opt. Mater. **34**(8), 1371–1374 (2012).
21. J. Ito and H. Johnson, "Synthesis and study of yttrialite," Am. Mineral. **53**, 1940–1952 (1968).
22. R. Lo Savio, M. Miritello, A. M. Piro, F. Priolo, and F. Iacona, "The influence of stoichiometry on the structural stability and on the optical emission of erbium silicate thin films," Appl. Phys. Lett. **93**(2), 021919 (2008).
23. C. Jacinto, S. L. Oliveira, L. A. O. Nunes, T. J. Catunda, and M. J. V. Bell, "Energy transfer processes and heat generation in Yb^{3+}-doped phosphate glasses," J. Appl. Phys. **100**(11), 113103 (2006).
24. P. Yang, P. Deng, and Z. Yin, "Concentration quenching in Yb:YAG," J. Lumin. **97**(1), 51–54 (2002).
25. P. Cardile, M. Miritello, and F. Priolo, "Energy transfer mechanisms in Er-Yb-Y disilicate thin films," Appl. Phys. Lett. **100**(25), 251913 (2012).
26. B.-C. Hwang, S. Jiang, T. Luo, J. Watson, G. Sorbello, and N. Peyghambarian, "Cooperative upconversion and energy transfer of new high Er^{3+}- and Yb^{3+}-doped phosphate glasses," J. Opt. Soc. Am. B **17**(5), 833–839 (2000).
27. L. Zhang, H. Hu, C. Qi, and F. Lin, "Spectroscopic properties and energy transfer in Yb^{3+}/Er^{3+}-doped phosphate glasses," Opt. Mater. **17**(3), 371–377 (2001).
28. L. Laversenne, S. Kairouani, Y. Guyot, C. Goutaudier, G. Boulon, and M. T. Cohen-Adad, "Correlation between dopant content and excited-state dynamics properties in Er^{3+}–Yb^{3+}-codoped Y_2O_3 by using a new combinatorial method," Opt. Mater. **19**(1), 59–66 (2002).

1. Introduction

In the last decades, novel Er-doped Si-based light emitting materials received much attention, due to the possible applications as active media in devices for microphotonics [1,2]. Indeed erbium is chosen among the various luminescent centers, since it is characterized by a radiative emission at 1.54 μm, which represents a strategic wavelength for telecommunications, corresponding to a minimum loss of silica optical fibers [3]. Er-doped silica glass has been proposed as an efficient material for achieving optical gain, but in this matrix the total Er amount has to be limited to its solid solubility, which is usually low (~10^{19} Er/cm^3) [3]. Therefore, in order to achieve a reasonable gain in an active microphotonic device, like a waveguide planar amplifier, a long path is required [4,5]. Recently the scientific community tried to go beyond the doping by choosing materials, like Er oxide (Er_2O_3) [6,7] or Er disilicate ($Er_2Si_2O_7$) [8,9], in which Er could be incorporated with much higher contents, up to ~10^{22} Er/cm^3, thus acting as a major chemical component. In such cases all the Er ions are optically active, and therefore these materials were proposed for reducing the size and increasing the efficiency of planar optical amplifiers. However in such compounds Er-Er interactions are very strong, due to the very short Er-Er distance. In fact, the detrimental phenomena of concentration quenching and upconversion actually quench the Er luminescence, and cannot be avoided. An interesting compromise is given by mixed rare earth-based oxides [10,11] or silicates [12–16] in which the Er concentration can be tuned in a three orders of magnitude range, from 10^{19} Er/cm^3 to 10^{22} Er/cm^3, by diluting Er with other rare earth (RE) ions, such as the optically inactive Y, or the well-known sensitizer Yb. In these systems the Er-Er interactions can be perfectly tuned and controlled. In particular, very low cooperative upconversion coefficients were found in Y-Er and Yb-Er disilicates grown by magnetron co-sputtering [12,13,16]. Yttrium does not play any role in the Er luminescence, while ytterbium is demonstrated to increase the Er excitation cross section via Yb-Er energy transfer [17]. Additionally, the Yb-Er couple is often used in active media for fiber amplifiers

#175165 - $15.00 USD Received 28 Aug 2012; revised 13 Oct 2012; accepted 15 Oct 2012; published 29 Nov 2012
(C) 2013 OSA

[18] or lasers [19] and recently Yb-Er silicate was proposed as an active medium for electrically driven light emitting devices [20].

However, in such mixed rare earth compounds the disilicate stoichiometry forces the total amount of RE ions to be constant. Since the concentration of the single RE ion varies accordingly, it is not possible to achieve a control of the Yb:Er ratio. In order to overcome this limit, we start from Yb-Y disilicate thin films grown by magnetron cosputtering, and then we introduce Er by using ion implantation. This procedure leads to the formation of complex thin films, $Yb_xEr_yY_{2-x-y}$ disilicates, in which the concentrations of both active REs, Er and Yb, can be varied independently, in this way the Er sensitization from Yb ions can be effectively controlled. We will demonstrate that these films are stable, have a uniform distribution of the chemical components throughout their thickness and crystallize in the α-phase, which is the most optically efficient. Good optical properties will be reported by showing the efficient coupling between Yb and Er. We believe that these mixed disilicate thin films represent a valuable and promising approach for the realization of efficient planar amplifiers.

2. Experimentals

Yb-Y disilicate thin films, having different Yb concentrations, N_{Yb}, were grown by rf-magnetron cosputtering from three independent targets (Yb_2O_3, Y_2O_3 and SiO_2) on c-Si (100) substrates, heated at 400°C. All the films have the same thickness (about 160 nm), as measured by cross sectional SEM (Scanning Electron Microscopy) analyses, performed by using a Zeiss FEG-SEM Supra 25 Microscope. The atomic composition of the films was studied by Rutherford Backscattering Spectrometry (RBS), using a 2 MeV He^+ beam in random configuration, with a detector placed at 165° with respect to the incident beam. From RBS measurements we found that all the samples have always a disilicate composition, characterized by the ratio RE:Si:O = (Yb + Y):Si:O = 2:2:7, with Yb concentration spanning in a very extended range, between 1.7×10^{21} Yb/cm^3 and 1.5×10^{22} Yb/cm^3 (in the case of $Yb_2Si_2O_7$). After the growth, Er was introduced into the sample by ion implantation, using a 400 keV HVEE ion implanter. Two doses were implanted at 230 keV, namely 7.5×10^{15} Er/cm^2 and 2.3×10^{16} Er/cm^2. The samples were then thermally treated by performing a rapid thermal annealing (RTA) at 1200 °C for 30 s in O_2 ambient. This allowed the optimization of the film stoichiometry and induced the crystallization [12,13].

The crystalline structure was evaluated by X-Ray Diffraction (XRD) analyses, performed with a Bruker-AXS D5005 diffractometer, by using Cu Kα radiation at 1.54 Å, with a grazing incidence angle of 1.0°. The diffraction angle 2θ was varied between 18° and 36°.

Atomic Force Microscopy (AFM) analyses were performed with a Veeco-Innova microscope operating in contact mode. Ultra-sharpened Si tips were used (MSNL-10 from Veeco Instruments, with anisotropic geometry, radius of curvature 2 nm, tip height 2.5 micron, front angle 15°, back angle 25°, side angle 22.5°) and substituted as soon as a resolution loose was observed during the acquisition. The AFM images were analyzed by using the SPM Lab Analyses V7.00 software.

Finally, we observed the optical properties of the films by performing photoluminescence spectroscopy (PL), by exciting with a Ti:Sapphire tunable laser (between 700 nm and 1000 nm) chopped by an acousto-optic modulator. The PL intensity was dispersed in wavelength by a monochromator and then detected with a Ge photodetector; the overall signal/noise ratio is maximized by using a lock-in amplifier. We also performed time-resolved measurements by detecting the modulated PL signal with a Hamamatsu photomultiplier tube and then by analyzing the signal with a photon counter multichannel scaler, with a time resolution of ~100 ns.

3. Structural characterization

In this section we report the structural properties of the Er-implanted Yb-Y disilicate thin films. RBS measurements have permitted to estimate the stoichiometry of the as deposited

#175165 - $15.00 USD Received 28 Aug 2012; revised 13 Oct 2012; accepted 15 Oct 2012; published 29 Nov 2012
(C) 2013 OSA

Yb-Y silicate, always (Yb + Y):Si:O = 2:2:7, and the elemental concentration of each RE. Figure 1 reports the RBS spectra of two examples of Yb-Y silicate, restricted to the rare earths' signals. The RBS peaks associated to Y and Yb are well distinguishable and clearly indicate a uniform distribution of both components throughout the whole film thickness. Hence the Yb and Y contents have been estimated (for example, $N_{Yb} = 2.5 \times 10^{16}$ Yb/cm^2 and 1.2×10^{17} Yb/cm^2 are reported in the graph).

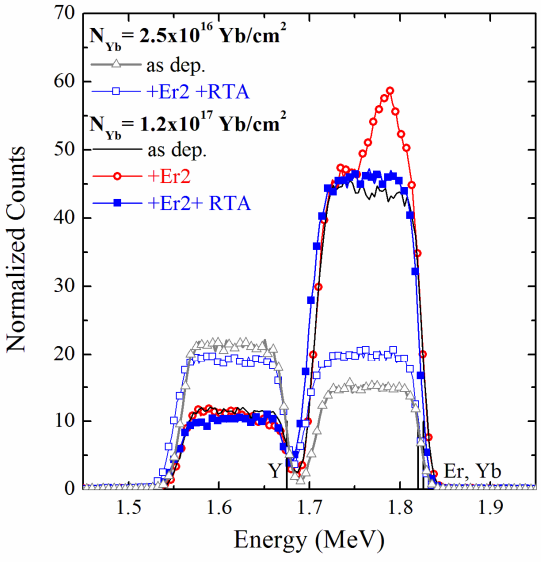

Fig. 1. RBS spectra of two examples of Yb-Y disilicate having different N_{Yb} content: as deposited, after implanting 2×10^{16} Er/cm^2 (Er2) and after implantation and RTA (Er2 + RTA). The threshold energies of Y, Er and Yb are also indicated.

In the same figure we also compared the REs RBS signals related to one sample, as an example, after implanting the highest Er dose studied in this paper, 2.3×10^{16} Er/cm^2, labeled as Er2. In the implanted film the Er RBS signal appears superimposed to the Yb one as a Gaussian peak, since Er and Yb have the very similar energy threshold, as reported in the same figure, owing to the similarities between their masses [12]. By subtracting the Yb peak of the unimplanted sample from the peak associated to the sum (Yb + Er) of the respective implanted one, an Er dose of 2.3×10^{16}/cm^2 is indeed confirmed. Moreover, after RBS measurements on all the as implanted samples, we found that the Er is totally located within the film, though it is not along the whole thickness.

In Fig. 1 we also reported the RBS spectra of the two examples of Yb-Y disilicate after the Er implantation and the following RTA treatment. It is worth noticing that after RTA the initial gaussian Er peak appears not visible in both cases. Moreover the (Yb + Er) RBS signal appears more intense with respect to the corresponding unimplanted case. In particular, its areal density is exactly equal to the (Yb + Er) peak related to the as implanted sample. Therefore we can certainly exclude that there was any RE outdiffusion from the film, but Er is now uniformly distributed throughout the whole film thickness. Besides, no interdiffusion of Si is observed at the interface. This is a clear indication that the films have a good stability on the Si substrate, even at very high temperatures, and that the Er ions have a strong mobility in the film during the annealing. We believe that this is due to the damage introduced in the matrix by the high dose ion implantation. It determines vacancy-like defects formation, which

#175165 - $15.00 USD Received 28 Aug 2012; revised 13 Oct 2012; accepted 15 Oct 2012; published 29 Nov 2012
(C) 2013 OSA

are supposed to favour the mobility of Er during the RTA treatment. Finally Er is well distributed along the whole thickness because it looks for oxygen, uniformly placed in the film, for optimizing its chemical surrounding. Note that even after implanting this high Er dose, the RBS spectra of all the implanted Yb-Y disilicates reveal that the film stoichiometry is still almost unchanged (RE:Si:O = (Y + Yb + Er):Si:O ≈2:2:7).

In order to estimate if there is also a change of the film density, which cannot be appreciated by RBS measurements, we have firstly measured the thickness of the as deposited Yb-Y films, about 160 nm (see the cross-sectional SEM image reported in Fig. 2(a)). Then we performed ion implantation of the film through a metallic grating, characterized by open squares 50 μm large, in order to keep a portion of the implanted area close to the unimplated one. After implantation we removed the grating and we performed AFM measurements. An AFM picture of the implanted sample is reported in Fig. 2(b), where the square regions, opened to the implantation, are clearly distinguishable, by demonstrating film thickness modification. In order to better evaluate the film modification, we analyzed in detail the region near to the interface between the implanted and unimplanted area, highlighted in the black area in Fig. 2(b). This region has been magnified and translated in a 3D picture in Fig. 2(c): it is immediately clear that the Er implantation makes the material more compact, reducing its thickness.

From a quantitative analysis, between the points indicated by red and green arrows corresponding respectively to the unimplanted and implanted region in Fig. 2(c) and in Fig. 2(d), it is evident a remarkable step height. After a statistical analysis on different squares, we estimated it 14.0 ± 2.0 nm. During implantation there are not re-sputtering phenomena from the surface due to the highly energetic implantation, as confirmed by the unchanged integral of the RBS rare earth peaks. We can hence conclude that the step height is due to a strong contraction of thickness, about 9%, in the implanted film in respect to the as deposited one; therefore the film appears clearly denser after ion implantation.

Since Er is uniformly distributed along the whole thickness after the thermal treatment, now it is possible to express the Er concentrations as expressed in Er/cm^3, i.e. obtained dividing the Er dose by the implanted film thickness. The two implanted doses then correspond to 5×10^{20} Er/cm^3 and 1.5×10^{21} Er/cm^3. This notation allows to easily compare the Er content with the Yb one, that will be also expressed in Yb/cm^3, varying between 1.7×10^{21} Yb/cm^3 and 1.5×10^{22} Yb/cm^3. Note that in the case of Yb content we will refer to the same Yb volume density between the unimplanted and implanted samples, though in the second case it is slightly larger owing to the thickness reduction after implantation. It is possible because this difference does not influence the structural and optical evolution.

#175165 - $15.00 USD Received 28 Aug 2012; revised 13 Oct 2012; accepted 15 Oct 2012; published 29 Nov 2012
(C) 2013 OSA

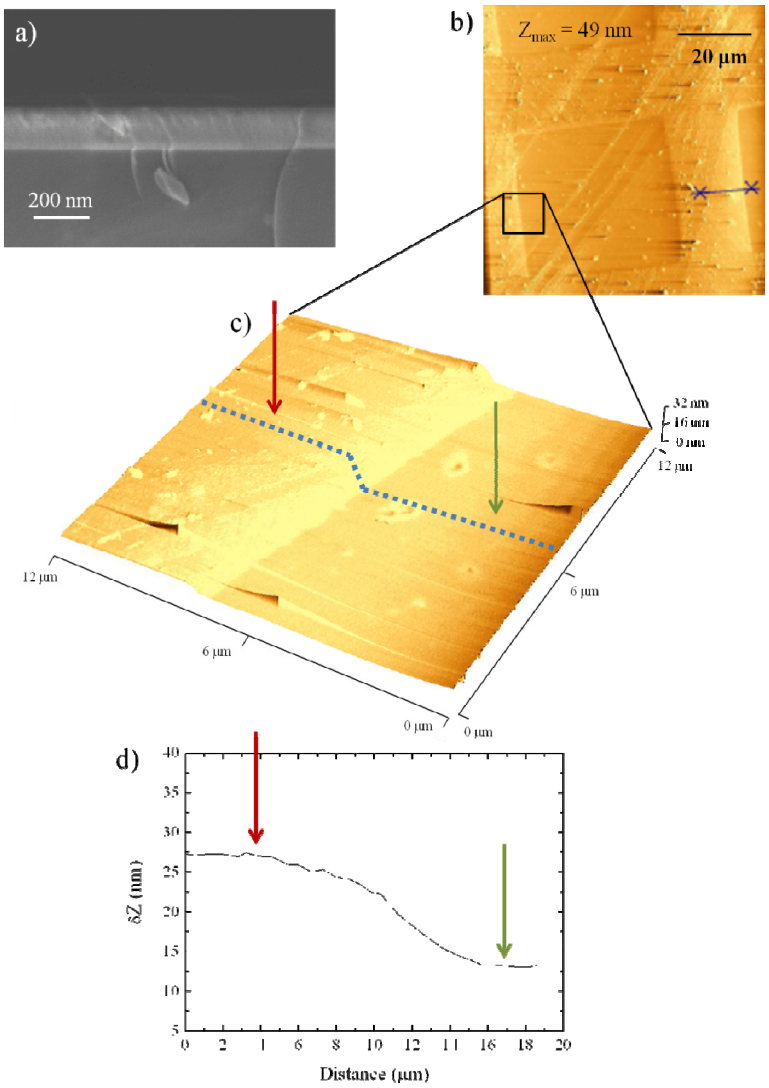

Fig. 2. (a) Cross sectional SEM image of an as deposited Yb-Y disilicate. (b) AFM measurements on an as-implanted sample, after removing a masking grating. (c) AFM zoom-in reporting the step height in a 3D picture. (d) Analytical measurement of the step height.

In order to analyze the effect of the erbium implantation in the film crystallization properties, we performed the same thermal treatment (1200°C, 30s, O_2) of all the as-deposited and as-implanted disilicate samples. In Fig. 3 we compare the XRD spectra, for all the investigated Yb contents with and without Er, in the range of diffraction angle, 2θ, between 18° and 36°. The same narrow and intense diffraction peaks characterize all the spectra, thus confirming that crystallization occurred after the thermal treatment in all the cases. These peaks can be associated to two different polymorphs of rare earth disilicates, namely y- and α-phases, (diffraction patterns JCPDS database no. 74-1994 and 38-0223, respectively, related to $Y_2Si_2O_7$) as reported in the legend of the graph. For the samples without Er (continuous lines) we noticed that there is a slight shift of the diffraction peaks towards higher 2θ, by increasing the Yb concentration. This happens for both the polymorphs, and it is clearly due to a shrinking of the lattices, since the Yb ions are substituting the Y ones in the lattice and the ionic radius of Yb (0.86 Å) is smaller than the Y one (0.90 Å) [21].

#175165 - $15.00 USD Received 28 Aug 2012; revised 13 Oct 2012; accepted 15 Oct 2012; published 29 Nov 2012
(C) 2013 OSA

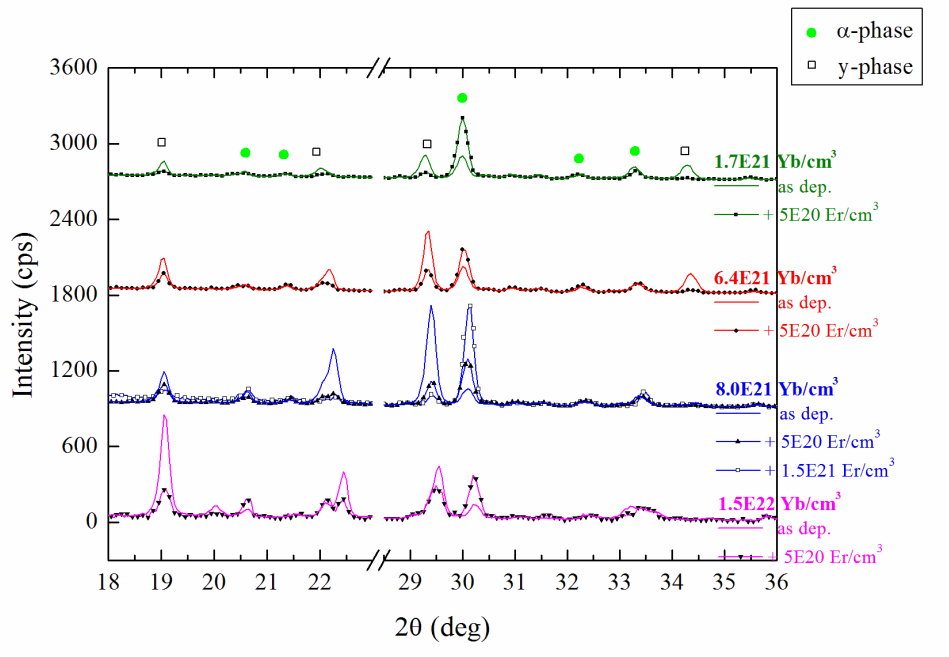

Fig. 3. Comparison of the XRD spectra of the Yb-Y disilicates after thermal treatment for all the N_{Yb} values investigated (continuous lines), and after 5×10^{20} Er/cm^3 implantation (lines and full symbols). For the sample with 8.0×10^{21} Yb/cm^3, the XRD spectrum related to the higher implanted Er dose, 1.5×10^{21} Er/cm^3, is also reported (line and open symbols).

When Er is implanted (line and full symbols in Fig. 3), no further shift is observed but a significant effect on the relative intensities of the peaks is present for all the N_{Yb} values. Particularly all the peaks related to the y-phase become less intense in favor of the ones associated to the α-phase. Moreover by increasing the Er content from 5×10^{20} Er/cm^3 to 1.5×10^{21} Er/cm^3, a further relative increase of the α-phase peaks is registered. This is true for all the samples, but for the sake of simplicity it is shown only for $N_{Yb} = 8.0 \times 10^{21}$ Yb/cm^3 in Fig. 3. The effect is particularly evident by looking at the two main peaks of the y- and α- phases, at 29.5° and 30.5° respectively. There is a simple explanation for this effect. As stated previously, the damage introduced by ion implantation may correspond to a strong local mobility for Er. Since it is known that the α-phase crystallizes at higher temperatures with respect to the y-phase [21], we can deduce that the α-phase could be favored during crystallization of the implanted samples as a result of the higher atomic mobility. Note that the α-phase has the highest tabulated atomic density (8.7×10^{22} at/cm^3 for α-$Yb_2Si_2O_7$, according to JPCDS no. 030-1439), about 9% higher than all the other disilicate polymorphs (see for example 7.8×10^{22} at/cm^3 for y-$Y_2Si_2O_7$, according to JPCDS no. 74-1994). This further explains why ion implantation determines a denser material, having the same 9% of thickness reduction. In summary ion implantation determines a more homogeneous crystalline phase with a much higher presence of the α-phase. This would remove the problem of grain borders, possibly reducing the scattering losses and increasing the performances of a waveguide amplifier. Moreover it has been demonstrated that the α-phase is the most efficient for Er-based disilicates from the optical point of view [22].

4. Optical characterization

We characterized the optical properties of the Er-doped Yb-Y disilicate thin films, both with PL spectroscopy and time-resolved measurements. We excited them at 935 nm, a wavelength

#175165 - $15.00 USD Received 28 Aug 2012; revised 13 Oct 2012; accepted 15 Oct 2012; published 29 Nov 2012
(C) 2013 OSA

at which Yb absorbs very efficiently, owing to its $^2F_{7/2} \rightarrow {}^2F_{5/2}$ transition and not resonant with any Er levels. Therefore only Yb can be directly excited at this wavelength [12].

After RTA treatments all the implanted samples show an intense luminescence peaked at 1.54 μm having the same PL shape. Figure 4(a) reports some of the recorded PL spectra, they have the typical shape obtained from Er ions in α-disilicate environment [11]. By comparing the samples implanted with the two Er doses, it is evident that the PL intensity has two opposite trends as a function of N_{Yb}. For the lower Er concentration (5×10^{20} Er/cm^3) the maximum PL intensity is reached for the lowest N_{Yb} investigated (1.7×10^{21} Yb/cm^3), corresponding to a ratio Yb:Er ≈3:1. Instead when the Yb concentration is increased by a factor of 10, the Er PL intensity has been halved and the Yb PL emission has only a slight increase (less than 10%, data not shown). In this low Er regime the Er concentration is so small that, for all Yb contents, Yb-Yb interactions are favoured with respect to Yb-Er interaction. By increasing Yb content the Yb-Yb interactions [23,24] will increase and these might lead to the detrimental concentration quenching in which the excitation is finally lost in a quenching center. Therefore instead to transfer energy to Er ions – thus contributing to PL emission at 1.54 μm – the excited Yb ions interact each other and then de-excite non radiatively in quenching centers, as confirmed also by the Yb-PL decrease at 980 nm and this effect increases with increasing Yb concentration.

For the higher implanted Er dose (1.5×10^{21} Er/cm^3) the PL intensity for the minimum Yb content of 1.7×10^{21} Yb/cm^3 is the same of the one optimized for lower Er dose. However, in this case the number of sensitizers is still low with respect to the acceptors (Yb:Er ≈1:1). In fact, by increasing the Yb:Er ratio the Er PL emission increases and it reaches its maximum for $N_{Yb} = 1.5 \times 10^{22}$ Yb/cm^3. This can be associated to an increase of the Yb-Er transfer efficiency with respect to the competing process of the concentration quenching of the Yb network itself [24,25]. Therefore the transfer efficiency is demonstrated to be optimized when the population ratio between sensitizers and acceptors is Yb:Er ≈10:1 for 1.5×10^{21} Er/cm^3 [12], concentrations which are very high compared to those typically used in Yb-Er codoped materials [12,15–18].

This behaviour clearly demonstrates that the optimized coupling Yb:Er varies depending on both the rare earths' concentrations: in fact, the highest Er emission can be obtained if the Yb-Er transfer rate overcomes the other competing intrinsic Yb decay rates.

This result is true, providing that in all the cases there is an equivalent Er excitation cross section through the Yb ions. In order to verify this, we compared the Er emission by exciting at 935 nm and at 980 nm. It is worth noticing that the Er PL emission under 935 nm is proportional to the excitation cross section due to the sensitization process. On the other hand the Er PL emission under 980 nm can be due both to the sensitization and to the direct absorption from Er, since this wavelength is resonant also with the $^4I_{15/2} \rightarrow {}^4I_{11/2}$ transition (see inset of Fig. 4(b)). Note however that the direct Er absorption cross section is one order of magnitude lower than that one of Yb direct absorption [17]. Therefore the normalized ratio PL (λ_{exc} = 935 nm) / PL (λ_{exc} = 980 nm) recorded at 1.54 μm represents the percentage of the Er excitation contribution due to the Yb-Er sensitization with respect to all the excitation mechanisms. We reported this normalized ratio as a function of N_{Yb} in Fig. 4(b), for both implanted Er doses: for all the cases, we found that the mediated contribution is ≈100%. It means that the PL emission from Er ions under 980 nm for all the samples is totally due to the sensitization of the nearby Yb ions. This is an important result, since it confirms the efficient coupling Yb-Er even by varying N_{Yb} by two orders of magnitude, between 1.7×10^{21} Yb/cm^3 and 1.5×10^{22} Yb/cm^3, and with N_{Er} up to 1.5×10^{21} Er/cm^3.

#175165 - $15.00 USD Received 28 Aug 2012; revised 13 Oct 2012; accepted 15 Oct 2012; published 29 Nov 2012
(C) 2013 OSA

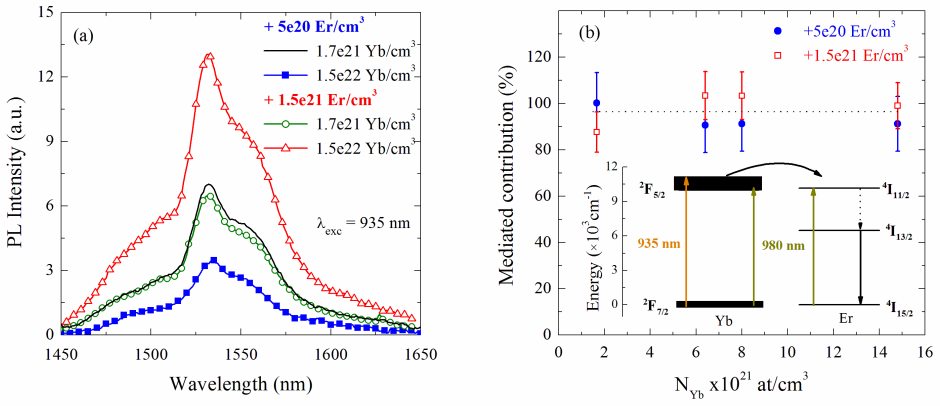

Fig. 4. (a) PL emission from Er at 1.54 μm, for both the implanted Er doses, and for the extreme values of N_{Yb}. (b) Percentage of the mediated contribution in the Er excitation via Yb-Er energy transfer. The inset reports a scheme of the Yb and Er energy levels involved.

The very efficient Yb-Er coupling suggests the absence of energy back-transfer processes [26] from Er to Yb. Since in the silicate host the phonon energy is so high to make the de-excitation $^4I_{11/2} \rightarrow {}^4I_{13/2}$ very fast, the population of $^4I_{11/2}$ quickly fills the $^4I_{13/2}$ level. But if the energy back-transfer rate from Er to Yb becomes competitive with the $^4I_{11/2} \rightarrow {}^4I_{13/2}$ relaxation, the $^4I_{13/2}$ population would reduce [27,28]. In order to evaluate this aspect we have compared the optical properties of the optimized sample containing Yb (1.5×10^{21} Er/cm^3 and 1.5×10^{22} Yb/cm^3) with that one of a Y-Er disilicate containing the same amount of Er but where the Yb ions are substituted with the optically inactive Y ions. The PL intensity and the lifetime at 1.54 μm, under 980 nm excitation, have been compared in Fig. 5(a) and Fig. 5(b) respectively.

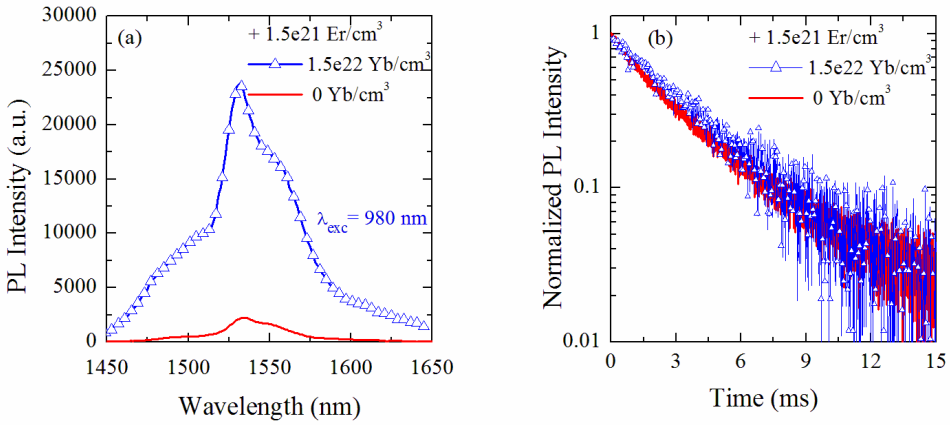

Fig. 5. (a) PL emission and (b) time resolved PL decay from Er at 1.54 μm in the implanted Yb-Y disilicate and in absence of Yb in Y-Er disilicate, for the same $N_{Yb} = 1.5 \times 10^{22}$ Yb/cm^3.

It is evident that while the PL intensity at 1.54 μm increases by one order of magnitude in the Yb-Y-Er disilicate, the decay times are identical. The lifetime, estimated as 5.3 ms by single exponential fit, is very long, considering the amount of Er present in the films. The similarities of the Er de-excitation in the two cases demonstrate that it is independent of the Yb presence, by confirming that the matrices are very similar. Instead the increase by a factor

#175165 - $15.00 USD Received 28 Aug 2012; revised 13 Oct 2012; accepted 15 Oct 2012; published 29 Nov 2012
(C) 2013 OSA

of 10 of the PL intensity at 1.54 μm, together with the demonstration of 100% mediated contribution (Fig. 4) at this excitation condition, demonstrates that the excitation cross section is increased by a factor of 10 when Yb ions are present. This factor corresponds to the ratio between Yb absorption cross section (2.0×10^{-21} cm^2) and that one of Er (2.0×10^{-20} cm^2), thus suggesting that Er excitation cross section corresponds exactly with the Yb absorption cross section in presence of Yb. Therefore this is another confirmation of the efficient of Yb-Er coupling in the investigated Er implanted Yb-Y disilicate.

5. Conclusions

We synthetized a new class of thin materials, highly Er-doped Yb-Y disilicate thin films, by performing and controlling their structural properties. After RTA the chemical components of the films are uniformly distributed in the whole thickness, thanks to the high Er mobility induced by implantation. Moreover, after implantation the films are characterized by a predominant crystallization in the α-phase, which optimizes the Er optical emission in a disilicate host. We verified that this crystallization can be ascribed to a densification of the material and to the high mobility locally introduced by ion implantation.

Finally we analyzed the optical properties of these films. Er is perfectly introduced in the host and it is characterized by a strong PL emission, due to the Yb-Er energy transfer mechanism. In fact, we demonstrated that the Er PL emission, for all the N_{Yb} investigated, is totally due to the sensitization of the nearby Yb ions and that no deleterious energy back-transfer occurs.

Owing to their structural and optical properties, this new class of thin films appears promising for the realization of planar optical amplifiers and active waveguides for applications in microphotonics.

Acknowledgments

The authors wish to thank G. Franzò and L. Romano and M. G. Grimaldi for useful discussions, C. Percolla and S. Tatì for expert technical assistance.

#175165 - $15.00 USD Received 28 Aug 2012; revised 13 Oct 2012; accepted 15 Oct 2012; published 29 Nov 2012
(C) 2013 OSA